JOURNAL OF GEOPHYSICAL RESEARCH, VOL. 103, NO. C6, PAGES 12,795–12,805, JUNE 15, 1998

Bound and free infragravity waves in the nearshore zone under breaking and nonbreaking conditions

B. G. Ruessink

Institute for Marine and Atmospheric Research Utrecht, Department of Physical Geography
Utrecht University, Utrecht, Netherlands

Abstract. Recordings of near-bottom pressure obtained at three positions in a gently sloping multiple-bar system were analyzed with a bispectral technique to quantify the relative importance of forced motions to the total infragravity (0.004 - 0.04 Hz) wave field under breaking and nonbreaking conditions, both on a temporal and spatial scale. The temporal variations in the ratio of bound to total infragravity energy E_{bnd}/E_{ig} were well associated with the local relative wave height H_{ss}/h (where H_{ss} is the significant sea-swell wave height and h is water depth). E_{bnd}/E_{ig} increased with higher H_{ss}/h values, reaching maximum values of up to 0.8 at the onset of short-wave breaking. With an increasing intensity of breaking the coupling between incident and infragravity waves reduced to negligible values in a saturated sea-swell wave field. The strong phase coupling at the breakpoint with a phase relationship close to the relationship predicted by bound-wave theory strongly supports the hypothesis that forced waves are the main source of free infragravity motions. In the cross-shore direction, E_{bnd} was largest at the breakpoint. Wave breaking was associated with a rapid decrease in the ratio E_{bnd}/E_{ig} in the onshore direction and, consequently, with a rapid increase in the contribution of free infragravity energy to the total infragravity field. The data set indicated that free infragravity energy may also be generated in the absence of breaking waves; the reason for this is not understood.

1. Introduction

Since the initial observations of surf beat by *Munk* [1949] and *Tucker* [1950], much effort has been devoted to investigate the source of these motions (also called infragravity or long waves) with typical frequencies of 0.004 - 0.04 Hz. In general, infragravity-wave energy is highly correlated to energy in the short-wave frequency band (typically 0.04 - 0.33 Hz) [e.g., *Elgar et al.*, 1992; *Okihiro et al.*, 1992], indicating that the long-wave motions are locally driven by incident sea and swell. It is believed that free infragravity waves are surf zone generated, related to the breaking of the incident short-wave groups in shallow water. In spite of this, little direct observational evidence based on field measurements has been presented in the literature to confirm this hypothesis. Especially, the effect of short-wave breaking on the composition of the infragravity-wave field is unknown, and as a result, the generation of infragravity motions is still not well understood.

Theoretically, pairs of short waves with frequency f and $f+\Delta f$ (where Δf is in the infragravity-frequency band) nonlinearly excite secondary bound long waves with difference-frequency Δf [*Hasselmann*, 1962; *Longuet-Higgins and Stewart*, 1962]. Although the effect of short-wave breaking on these nonlinear interactions is unknown, it has been hypothesized that the incident bound long waves are not destroyed in the surf zone but are released as free waves [*Longuet-Higgins and Stewart*, 1962]. After reflection at the shoreline the released wave motions propagate in a seaward direction and may either escape into deep water (i.e., leaky waves) or remain refractively trapped to the shore (i.e., edge waves [see, e.g., *Herbers et al.*, 1995a]). Recent investigations in intermediate water depths (roughly 8 - 30 m), well outside the surf zone, have actually demonstrated that the total infragravity wave field consists of a mixture of bound and free wave motions [*Bowers*, 1992; *Elgar et al.*, 1992; *Okihiro et al.*, 1992; *Herbers et al.*, 1994, 1995b]. As shown in these studies, forced waves become a more substantial part of the total long-wave field with increasing short-wave energy (and thus total infragravity energy) and decreasing water depth. Most field experiments carried out inside the surf zone have indicated that energy in the infragravity band is primarily associated with free wave motions [e.g., *Holman*, 1981; *Huntley et al.*, 1981; *Howd et al.*, 1991; *Oltman-Shay and Guza*, 1987]. For instance, *Huntley et al.* [1981] reported that low-mode edge waves contributed significantly to the longshore currents at infragravity frequencies, whereas high-mode edge waves and leaky waves tended to prevail in the onshore/offshore currents. Their data set further indicated that forced wave motions might add to the cross-shore motions at infragravity frequencies, although they did not quantify the bound-wave contribution. Presumedly, the ratio of bound to total long-wave energy is largest at the onset of short-wave breaking.

An alternative model for the generation of low-frequency energy at the breakpoint is that of *Symonds et al.* [1982], in which the time-varying position of the breaker line induced by the group structure of the incident short waves results in setup oscillations on the timescale of the incident wave

Copyright 1998 by the American Geophysical Union.

Paper number 98JC00893.
0148-0227/98/98JC-00893$09.00

groups. The relative importance of the two mechanisms to free infragravity-frequency generation is unknown. However, the propagation characteristics of infragravity waves observed in 13 m depth by *Herbers et al.* [1995a] were consistent with the nonlinear generation of these waves in shallow water, suggesting that the release of bound infragravity waves is the main source of free long-wave motions.

It is the aim of the present paper to describe results of a field experiment that yielded quantitative information about the composition of the infragravity-wave field under breaking and nonbreaking conditions, both on a temporal and spatial scale. The outline of this paper is as follows. After a description of the field site and the observations in section 2 the bispectral method that was applied to estimate the local coupling between incident sea-swell and infragravity-wave energy is presented in section 3. In the first part of section 4 the temporal variations in forced and free infragravity energy are shown as a function of the offshore short-wave energy and the local short-wave height normalized by depth. In the second part a closer look is taken at the cross-shore evolution of the different constituents in the total infragravity wave field. The discussion is presented in section 5, followed by a summary of the main conclusions in section 6.

2. Field Site and Observations

Wave data were collected at three cross-shore positions in section 17 at Terschelling, Netherlands, during the 1993/1994 winter. The field site is located on the seaward side of the approximately 30-km-long barrier island Terschelling, which borders a wide (several hundreds of kilometers) shallow shelf (North Sea). The nearshore morphology at the start of the campaign and the three instrumented positions labeled P1, P2, and P3 are shown in Figure 1a. The field site is characterized by three bars [see also *Ruessink and Kroon*, 1994]. A shoreface nourishment, which is clearly visible in Figure 1a as an area with an irregular surface between kilometersections 14 and 18, was implemented in the outer trough about half a year prior to the start of the campaign [*Hoekstra et al.*, 1994]. As can be seen more clearly in Figure 1b, P1 and P3 were positioned on the seaward flank of the outer bar and on the crest of the middle bar, respectively. The mean water depths at these positions were 5.2 m and 3.7 m, respectively. P2 was located in the intermediate trough at a mean water depth of 5.1 m. The median grain size at the measurement positions is about 180 μm. The tidal range at the field site ranges between 1.2 m and 2.5 m at neap and spring tide, respectively.

A pressure transducer was positioned at 2 m above the bed at P1 and P3 and at 4 m at P2. Recordings were continuously performed with a sampling rate of 2 Hz at P1 and P3 and of 4 Hz at P2. Unfortunately, data were not always collected simultaneously at all three locations owing to several technical problems. The available records were split into 136-min-long sections. All time series that showed nonstationarities (e.g., in water level, variance, peak frequency, etc.) were rejected from the present analysis. A total of 62, 33, and 20 series were selected for analysis at P1, P2, and P3, respectively. All these time series were either collected around high or low water. The selected data spanned a wide range of offshore wave conditions, which were measured by a directional wave buoy at 15-m water depth roughly 5 km from the shore. The offshore significant wave height $H_{ss,o}$, defined as $4E_{ss,o}^{0.5}$, where $E_{ss,o}$ is the offshore short-wave variance in the frequency band from 0.03 to 0.5 Hz, ranged from 0.25 m to 6.2 m. The offshore significant period, calculated with a standard zero-downcrossing technique in the time domain, varied between 5 and 13 s.

The infragravity-frequency band was defined as 0.004 to 0.04 Hz. Frequencies below 0.004 Hz were not considered, because the log of the spectral levels at these frequencies and the log of the total energy integrated over the 0.05- to 0.33-Hz band were, in general, weakly correlated, implying that these very low frequency motions were not always short-wave driven. The upper frequency boundary of the infragravity band was set to 0.04 Hz to ensure that infragravity energy levels were not contaminated by occasionally incident very high period swell. The short-wave frequency band was taken as 0.04 - 0.33 Hz.

In the present paper the relative wave height, defined as the ratio between local significant short-wave height and water depth H_{ss}/h, is applied to investigate whether or not a position experienced breaking conditions. To calculate H_{ss}, the short-wave frequency band of the pressure spectrum was converted to free surface elevation with a depth correction using linear wave theory. *Van Enckevort and Reincke* [1996] made extensive measurements of wave heights in the intertidal zone with a bottom slope of 1:100 at the Terschelling field site. During most of their measurements they noted whether waves were breaking. They found that virtually all observations labeled as nonbreaking had H_{ss}/h values of less

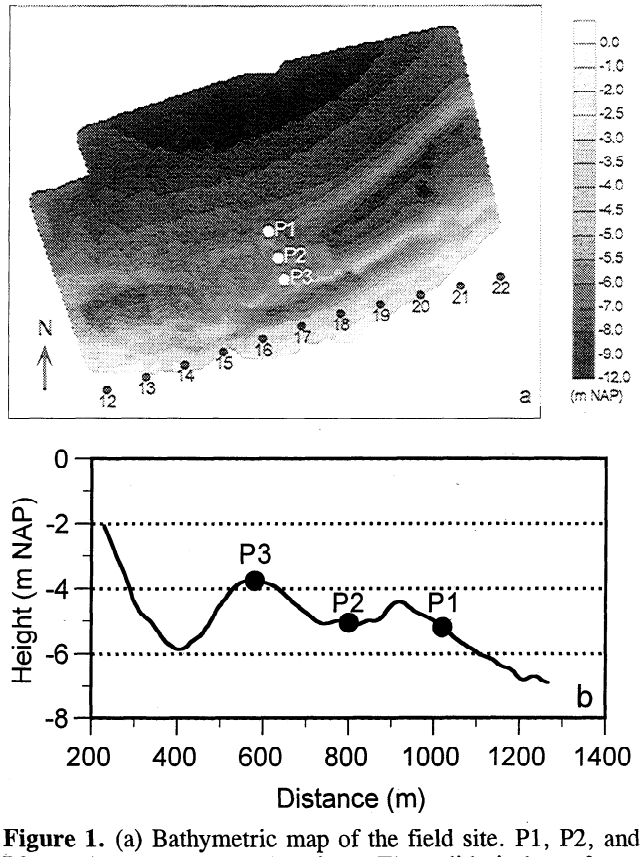

Figure 1. (a) Bathymetric map of the field site. P1, P2, and P3 are the measurement locations. The solid circles refer to kilometersections. The cross-shore distance is exaggerated 3 times with respect to the longshore distance to stress the barred morphology. Height is with respect to Dutch ordnance level (NAP) (0 m NAP is about mean sea level). (b) Cross-shore profile of the measurement section (17).

than 0.33, whereas surf zone conditions were associated with H_{ss}/h values in excess of 0.33. The H_{ss}/h value of 0.33 thus seems to mark the onset of breaking at the Terschelling site. As this value corresponds to the breaking of the highest waves in a wave group, H_{ss}/h rises with an increasing breaking intensity (i.e., more breaking waves); it reaches a maximum value (often referred to in the literature as γ) when all waves are broken and the energy is thus saturated [*Thornton and Guza*, 1982]. The largest value observed by *Van Enckevort and Reincke* [1996] amounted to 0.59. In troughs, such as at P2, the applicability of H_{ss}/h may be restricted; here the relative wave height at the more seaward located bar crest may be a more suitable measure to determine whether P2 was inside the surf zone. However, data from the outer bar crest were absent, and as a consequence, H_{ss}/h at P2 was applied. Section 4 shows that this choice did not seriously affect the outcome of the analysis for P2.

In this paper the nomenclature of variables with respect to their measurement positions is as follows. The location code (P1, etc.) is added as a superscript to refer to a specific measurement position. Conversely, if this superscript is lacking, the variable refers to all locations simultaneously.

3. Observation of Bound Long Wave Energy

Bispectral analysis, introduced by *Hasselmann et al.* [1963], was applied to isolate the amount of bound from the total infragravity energy. In general, the bispectrum is described in the form of its normalized magnitude and phase, called bicoherence and biphase, respectively. The bicoherence $b(f_1,f_2)$ between wave components with frequencies f_1, f_2, and $f_1 + f_2$ is given as

$$b(f_1,f_2) = \frac{B(f_1,f_2)}{\left[E(f_1)E(f_2)E(f_1+f_2)\right]^{0.5}} \quad (1)$$

where $B(f_1,f_2)$ is the (dimensional) bispectral estimate and $E(f)$ is energy density. As can be seen in (1), $B(f_1,f_2)$ is normalized by the square root of the cross product of the energy densities at the three interacting frequencies. The biphase $\beta(f_1,f_2)$ is

$$\beta(f_1,f_2) = \arctan\left[\frac{\mathrm{Im}\{B(f_1,f_2)\}}{\mathrm{Re}\{B(f_1,f_2)\}}\right] \quad (2)$$

with $\mathrm{Im}\{B(f_1,f_2)\}$ and $\mathrm{Re}\{B(f_1,f_2)\}$ being the imaginary and real part of the bispectrum, respectively. In the present paper we are interested in the difference-frequency interactions of two primary swell-sea frequencies f and $f+\Delta f$ ($f_1 = f$, $f_2 = \Delta f$) contributing to $b(f,\Delta f)$ and $\beta(f,\Delta f)$. For free (Gaussian) wave fields the bicoherence is zero, but it becomes nonzero if phase coupling between wave triads exists. The statistics of bicoherence and biphase are not fully understood. Numerical simulations of nonlinear random harmonic processes (i.e., sum-frequency interactions) performed by *Elgar and Sebert* [1989] have indicated that the statistical uncertainty in the calculations is large when the bicoherence is low and/or the degrees of freedom are limited. The biphase then tends to be distributed randomly between -180° and 180° [e.g., *Elgar and Guza*, 1985]. With increasing nonlinearity and/or a large number of degrees of freedom (in general, long time series) the statistical uncertainty decreases and the biphase becomes stable. The time series in the present data set are of a sufficient length to expect that the bispectra uncertainties are generally low. The uncertainties for the present work are further discussed in section 4.

An estimate of the ratio of bound to total infragravity-wave energy at difference-frequency Δf can be obtained by integrating the bispectrum over all interactions involving this Δf (neglecting the contribution of those pairs with f_1 within the infragravity-frequency band). Subsequent integration over all possible difference-frequencies results in an estimate of the fraction of bound energy in the entire infragravity-frequency range [*Herbers et al.*, 1994]:

$$\frac{E_{bnd}}{E_{ig}} = |b_{ii}|^2 \quad (3)$$

where E_{bnd} and E_{ig} are bound and total infragravity energy, respectively, and b_{ii} is the double-integrated bicoherence. By substituting *Hasselmann et al.*'s [1963] theoretical expressions for $B(f,\Delta f)$ obtained by perturbation analysis into (1), *Herbers et al.* [1994] showed that the ratio between bound and total infragravity energy given by (3) has a small negative bias in intermediate water depths. This bias is caused by variations in the strength of interaction over contributing wave triads. In shallower water and under breaking-wave conditions, though, where the present measurements were made, bound-wave theory is known to become invalid, and no theoretical expression for bispectral values exists. Nevertheless, the bispectrum should still give some measure of phase coupling between infragravity and incident waves, and the ratio of bound to total infragravity energy is, therefore, estimated as $|b_{ii}|^2$, similar to that given by *Herbers et al.* [1994, 1995b]. As the statistical uncertainty in the estimate of bound energy at an individual difference-frequency Δf is considerably larger than in the total bound energy integrated over the entire infragravity-frequency band [*Herbers et al.*, 1994], only the latter one is shown in the present paper.

In the present investigation, estimates of (bi)spectra were obtained from Fourier transforms of detrended, 50% overlapping, and tapered data segments with a length of 2048 s (the length of an entire time series amounted to 136 min, see section 2). After frequency band merging the frequency resolution was 1/512 Hz. Prior to the analysis the measured spectra were converted to sea bottom pressure with the depth correction of linear wave theory to compensate for the different instrument positions in the vertical with respect to the total water depth. The forcing of short waves in the frequency band 0.25 - 0.33 Hz was neglected in the bispectral calculations; errors in the ratio of bound to total long-wave energy caused by this omission are presumably very small, as bound infragravity energy is mainly forced by short-wave pairs with frequencies close to the peak frequency [e.g., *Elgar and Guza*, 1985; *Herbers et al.*, 1994].

4. Results

4.1. Temporal Variations

The measured infragravity energy levels E_{ig} at P1, P2, and P3 were, as expected, well related to the offshore short-wave energy $E_{ss,o}$ (Figures 2a-2c). The straight lines through the points are the least squares fits through the logarithm of the data. The corresponding correlation coefficients r and slopes m are given in the upper part of Table 1 (note $E_{ig} \propto E_{ss,o}^{m}$). At each position, E_{ig} was about linearly related to $E_{ss,o}$ ($m \approx 1$). As can be deduced from Figures 2a-2c, short-wave breaking does not seem to alter the $E_{ss,o}$ dependence of E_{ig}.

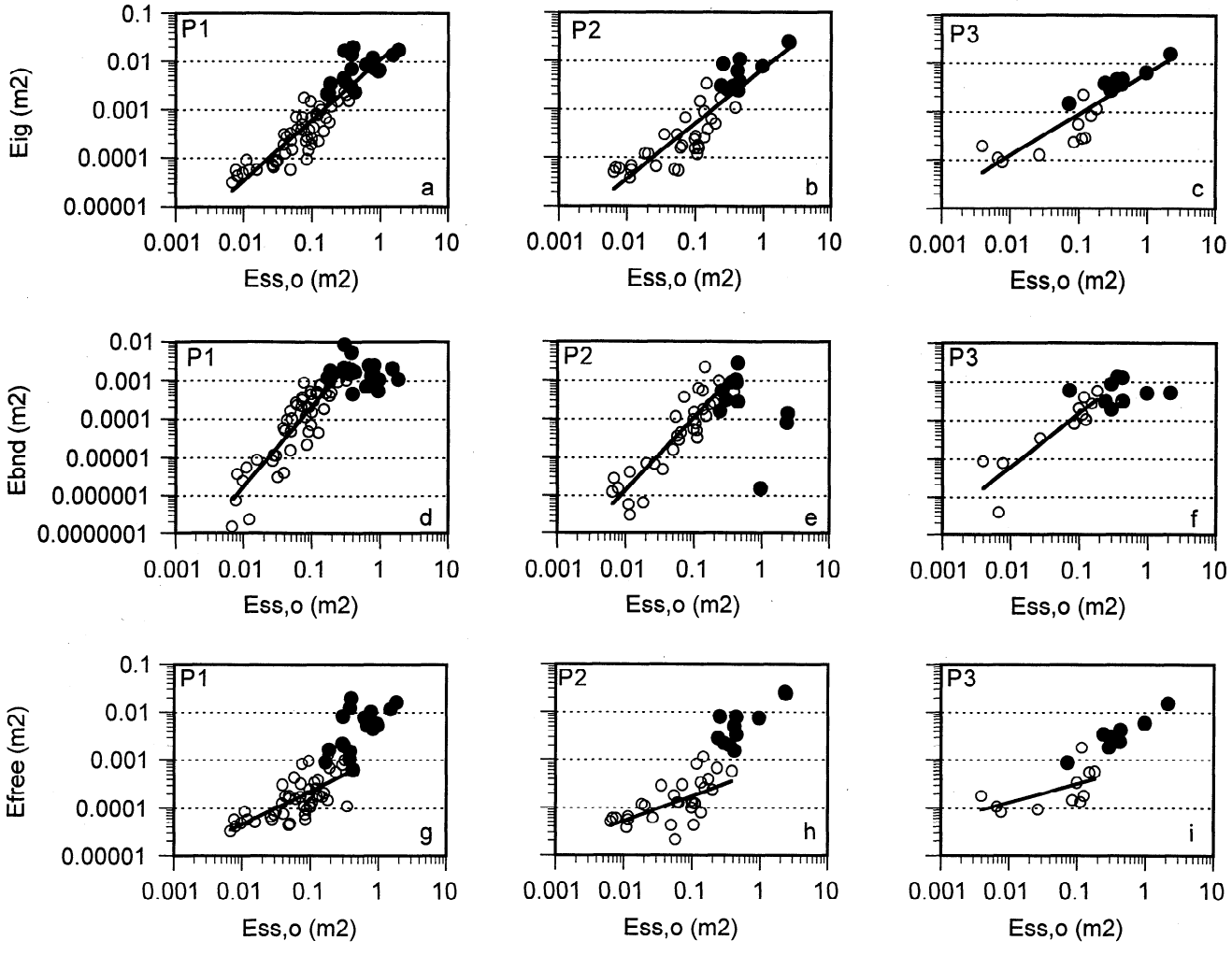

Figure 2. (top) Measured total, (middle) bound, and (bottom) free infragravity energy E_{ig}, E_{bnd}, and E_{free}, respectively, as a function of offshore short-wave energy $E_{ss,o}$ at (a), (d), and (g) P1, (b), (e), and (h) P2, and (c), (f), and (i) P3. Open and solid circles refer to nonbreaking and breaking conditions, respectively. The solid line in each plot is the best linear fit to the logarithm of the data (for E_{bnd} and E_{free} nonbreaking data only). The corresponding slopes m and correlation coefficients r are shown in Table 1.

Table 1. $E_{ss,o}{}^m$ dependence of E_{ig}, E_{bnd}, and E_{free}

Position	r	m	Number
		E_{ig}	
P1	0.91	1.2	62
P2	0.89	1.1	33
P3	0.88	0.9	20
		E_{bnd}*	
P1	0.89	2.1	43
P2	0.91	1.9	22
P3	0.89	1.4	11
		E_{free}*	
P1	0.70	0.70	43
P2	0.62	0.53	22
P3	0.59	0.39	11

All correlation coefficients were significant at the 0.05 confidence level.

*Only observations under nonbreaking conditions ($H_{ss}/h < 0.33$) were used for the regression analysis.

Figures 2d-2f show the observed bound long-wave energy E_{bnd} at P1, P2, and P3 as a function of the offshore short-wave energy $E_{ss,o}$. At every position, E_{bnd} increased drastically with $E_{ss,o}$ for $H_{ss}/h < 0.33$, whereas it remained constant or even reduced under short-wave breaking conditions despite the increase in offshore short-wave energy. Under nonbreaking conditions, E_{bnd} was approximately proportional to $E_{ss,o}$ squared (m = 1.9 - 2.1, middle part in Table 1), consistent with bound-wave theory [*Hasselmann*, 1962; *Longuet-Higgins and Stewart*, 1962]. The corresponding correlation coefficients (Table 1) were around 0.9. The reduced exponent at P3 (m = 1.4) is likely related to the limited number of observations under nonbreaking conditions, but it might also indicate a breakdown of bound long-wave theory in shallow water. Scatter around the least squares lines may be caused by variations in water depth and in short-wave directional characteristics and period.

The power m of the fit relating the amount of free long-wave energy under nonbreaking conditions to the short-wave energy ($E_{free} \propto E_{ss,o}{}^m$) was much smaller than the value of m = 2 observed for the E_{bnd} dependence on $E_{ss,o}{}^m$ (Figures 2g-

2i, lower part of Table 1). The exponent decreased from 0.70 at P1 to 0.39 at P3 (Table 1). These slopes are smaller than the approximately linear (m = 1) relationship between E_{free} and $E_{ss,o}$ observed by *Herbers et al.* [1995b] in water depths ranging between 8 and 30 m. At each position the amount of free infragravity energy under surf zone conditions was higher than expected on account of the least squares lines based on the nonbreaking observations. In other words, the arrest in growth in E_{bnd} (Figures 2d-2f) coincided with an enhanced increase in E_{free}, indicating a transformation from bound to free long-wave energy inside the surf zone. The same factors responsible for the observed scatter in E_{bnd} may determine the variability of E_{free} around its general trend. In addition, changes in beach morphology, resulting in different long-wave reflections from the water line, may affect the amount of free long-wave energy.

As can be seen in Figures 3a-3c, the fraction of bound long-wave energy at each position was well associated with the local relative wave height. Thus the temporal variations in E_{bnd}/E_{ig} at a given position seem to be well linked to the proximity to the breakpoint. In general, the ratio of bound to total infragravity energy was small ($E_{bnd}/E_{ig} < 0.1$) during low-energy conditions and increased with higher short waves and/or smaller depths (increasing H_{ss}/h) to reach maximum values at H_{ss}/h = 0.2 - 0.4. This confirms that at a given cross-shore position forced waves contribute most to the total long-wave field at the start of short-wave breaking. Strikingly, these maximum values decreased in the onshore direction from roughly 0.5 - 0.8 at P1 to 0.3 - 0.5 at P3. With a growing intensity of wave breaking the coupling between infragravity and short waves reduced. The data set indicated that all forced long-wave motions were released in a saturated short-wave field.

The biphases, shown in Figures 4a-4c plotted versus H_{ss}/h, were generally stable for $0.1 < H_{ss}/h < 0.5$, whereas they were more scattered for the remaining situations when the nonlinearities were weak ($E_{bnd}/E_{ig} < 0.1$ - 0.2). This scatter shows the large statistical uncertainties in the bispectral calculations when only a small amount of the total infragravity energy is nonlinearly sea-swell driven (see section 3). For $0.1 < H_{ss}/h < 0.5$ the biphase was in most cases within 10° of 170°, close to the theoretical value of 180° derived by *Longuet-Higgins and Stewart* [1962]. The biphase did not evolve systematically in the cross-shore direction, which contrasts with the reduction in biphase in decreasing water depths as observed by *Elgar and Guza* [1985] for selected short-wave frequency pairs. This contrast is likely related to the smaller water depths during Elgar and Guza's field experiments, as the increasing lag of the bound wave motions behind the short-wave envelope is most marked in very shallow water [see also *Bowers*, 1992; *List*, 1992].

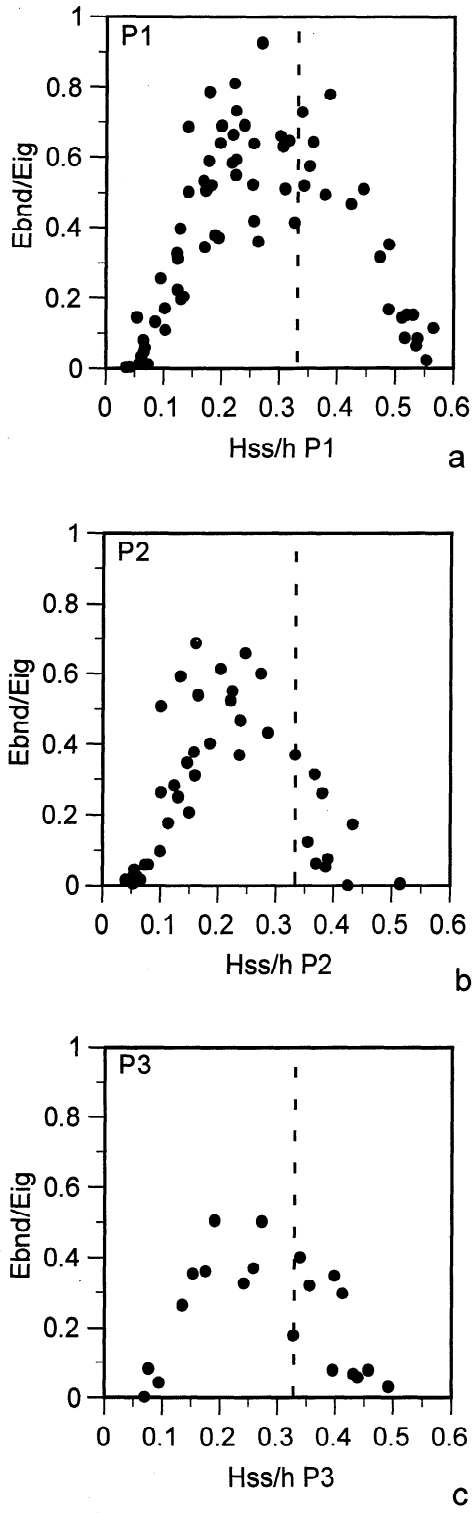

Figure 3. Observed ratio of bound to total infragravity energy E_{bnd}/E_{ig} as a function of relative wave height H_{ss}/h at (a) P1, (b) P2, and (c) P3. The dashed vertical lines mark the onset of wave breaking (H_{ss}/h = 0.33).

4.2. Cross-Shore Variations

The cross-shore amplification (i.e., ratio) of bound, free, and total long-wave energy between P1 and P2 is plotted against H_{ss}/h at P2 in Figure 5. As can be seen in Figure 5a, the amount of bound energy at P1 and P2 was about equal under nonbreaking conditions ($E_{bnd}^{P2}/E_{bnd}^{P1}$ scattered around 1). In contrast, E_{free} grew markedly ($E_{free}^{P2}/E_{free}^{P1} \approx$ 1.0 - 2.5) in the onshore direction when H_{ss}/h at P2 was less than 0.33 (Figure 5b). As a consequence, E_{ig}^{P2} was somewhat higher than E_{ig}^{P1} ($E_{ig}^{P2}/E_{ig}^{P1} \approx$ 1 - 1.5, Figure 5c) under these conditions. The reason for these trends is not fully understood. The increasing onshore growth in E_{free} with H_{ss}/h is unlikely related to an increase in trapping of free infragravity motions between P1 and P2. As P1 and P2 were located at approximately the same depth and were separated by the outer bar (Figure 1b), any free infragravity wave propagating onshore

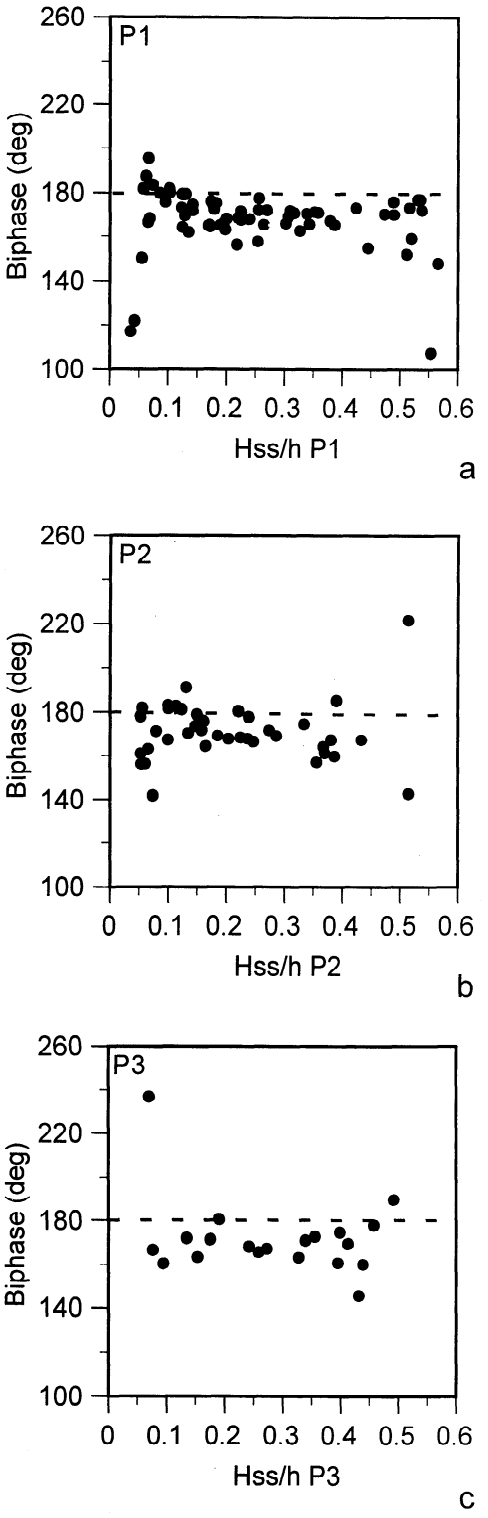

Figure 4. Observed biphase as a function of relative wave height H_{ss}/h at (a) P1, (b) P2, and (c) P3. The dashed horizontal lines denote the theoretical 180° biphase.

along P1 reaches P2, and similarly, any infragravity wave going offshore along P2 reaches P1, implying that free infragravity waves cannot be trapped between P1 and P2. Furthermore, a change in the degree of trapping would have implied a dependence of the directional characteristics of the free infragravity waves on the short-wave energy conditions, in contrast to *Herbers et al.*'s [1995b] observation that these characteristics are virtually independent of short-wave energy levels. A more feasible explanation is based on *Eldeberky and Battjes*'s [1994] laboratory findings. These authors ob-

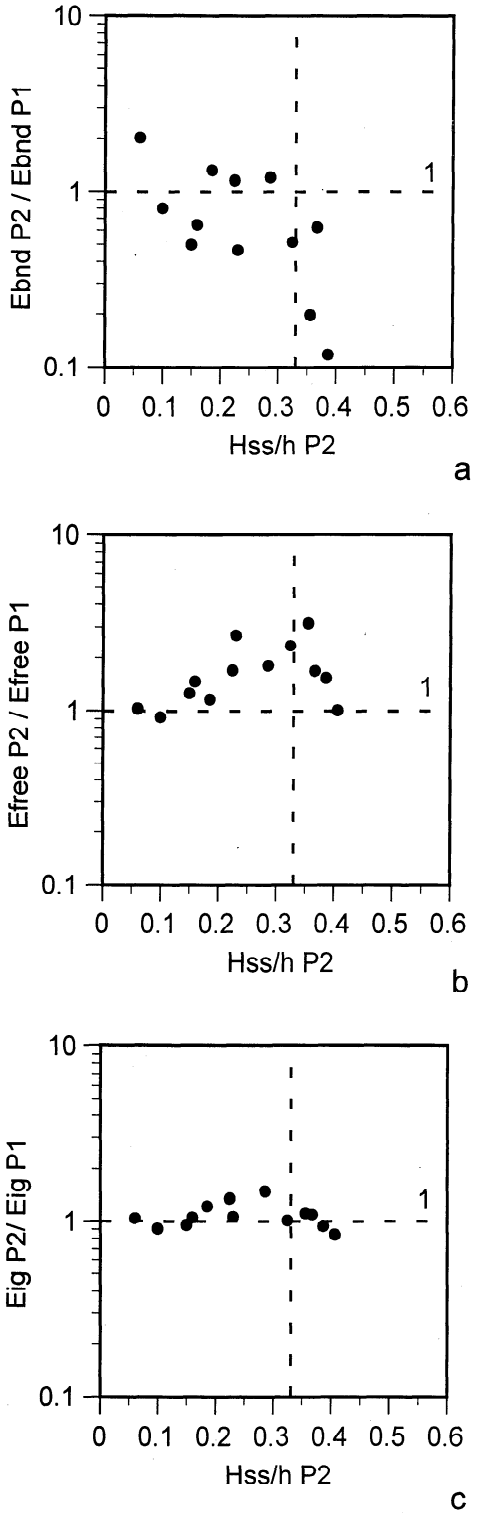

Figure 5. Cross-shore amplification of (a) bound, (b) free, and (c) total infragravity energy between P1 and P2 as a function of relative wave height H_{ss}/h at P2. The dashed vertical line in each plot denotes the onset of wave breaking (H_{ss}/h = 0.33). The horizontal dashed lines indicate equal amounts of energy at P1 and P2.

served a strong amplification of higher harmonics (sum-frequency interactions) in the shoaling region at the upsloping part of an artificial bar and a full release of these harmonics in the deepening part of the flume. During their experiments the waves passed the laboratory bar unbroken. Analogously, the forced infragravity energy levels may have increased from P1 toward the bar crest owing to the reducing water depth. When the long-wave field entered the trough, the degree of nonlinearity may have been reduced because of the greater water depth. This possibly caused an energy transfer from forced to free infragravity motions and, accordingly, resulted in values of $E_{free}^{P2}/E_{free}^{P1}$ and of E_{ig}^{P2}/E_{ig}^{P1} larger than 1. Obviously, this suggestion could have been more thoroughly checked if wave data had been collected at more positions over the outer bar. Nonetheless, Figures 5b and 5c indicate that E_{free} and E_{ig} increased between P1 and P2 in the absence of breaking waves.

Figure 6 shows the ratios of bound, free, and total infragravity energy at P3 to those at P1 as a function of the relative wave height at P3. The dashed horizontal line in Figure 6a represents the h^{-5} dependence equal to $(h^{P3}/h^{P1})^{-5}$ equal to 5.5 of forced infragravity energy, which, as shown by *Longuet-Higgins and Stewart* [1962], is the theoretical amplification in case of longshore uniformity and forcing by unidirectional, normally incident short waves. Finite-depth changes and directional effects are likely to reduce this value slightly [*Elgar et al.*, 1992]. The h^{-5} dependence was calculated for mean water situations (0 m NAP); at low (-1 m NAP) and high (+1 m NAP) water the theoretical onshore growth in E_{bnd} amounted to 9.1 and 4.0, respectively. The observed ratios of E_{bnd}^{P3} to E_{bnd}^{P1} were above 1 for nonbreaking conditions, but, in general, well below the theoretical h^{-5} dependence (Figure 6a). The onshore amplification of E_{bnd} decreased during more energetic situations. The reason of this is unknown. The lower dashed horizontal line in Figure 6b is the $h^{-0.5}$ dependence equal to $(h^{P3}/h^{P1})^{-0.5}$ equal to 1.2, the theoretical value for shoaling free normally incident (leaky) long waves. The upper dashed horizontal line shows the ratio $E_{free}^{P3}/E_{free}^{P1}$ in case of an isotropic directional spectrum (i.e., $E(\theta)$ = const, where θ is the propagation angle) at P3. According to Snell's law, seaward propagating long waves at oblique angle greater than about 60° are trapped shoreward of P1. The reverse shoaling of the remaining energy results in a value of 1.45 for the ratio $E_{free}^{P3}/E_{free}^{P1}$. Both ratios were calculated for mean water situations (0 m NAP); the differences between high and low water were small and are therefore not shown separately. For $H_{ss}/h \approx 0.2$ - 0.3, $E_{free}^{P3}/E_{free}^{P1}$ was well above what would be expected on account of the theoretical depth dependence of leaky waves and of the isotropical directional spectrum (Figure 6b), similar to the observations of $E_{free}^{P2}/E_{free}^{P1}$ (Figure 5b). It is likely that the generation of free long-wave energy that is not associated with short-wave breaking, as discussed in the previous paragraph, caused the onshore reduction in the maximum values of E_{bnd}/E_{ig} shown in Figure 3.

Interestingly, the total amount of infragravity energy decreased in the onshore direction during the most energetic situations shown in Figures 5c and 6c (both E_{ig}^{P2}/E_{ig}^{P1} and E_{ig}^{P3}/E_{ig}^{P1} were less than 1). This shoreward decrease in E_{ig} suggests that long-wave energy may be significantly damped during the breaking process of the incident sea and swell, although the precise mechanism remains unknown. Similar observations of long-wave damping were made by *Guza and Bowen* [1976] and *Eldeberky and Battjes* [1996].

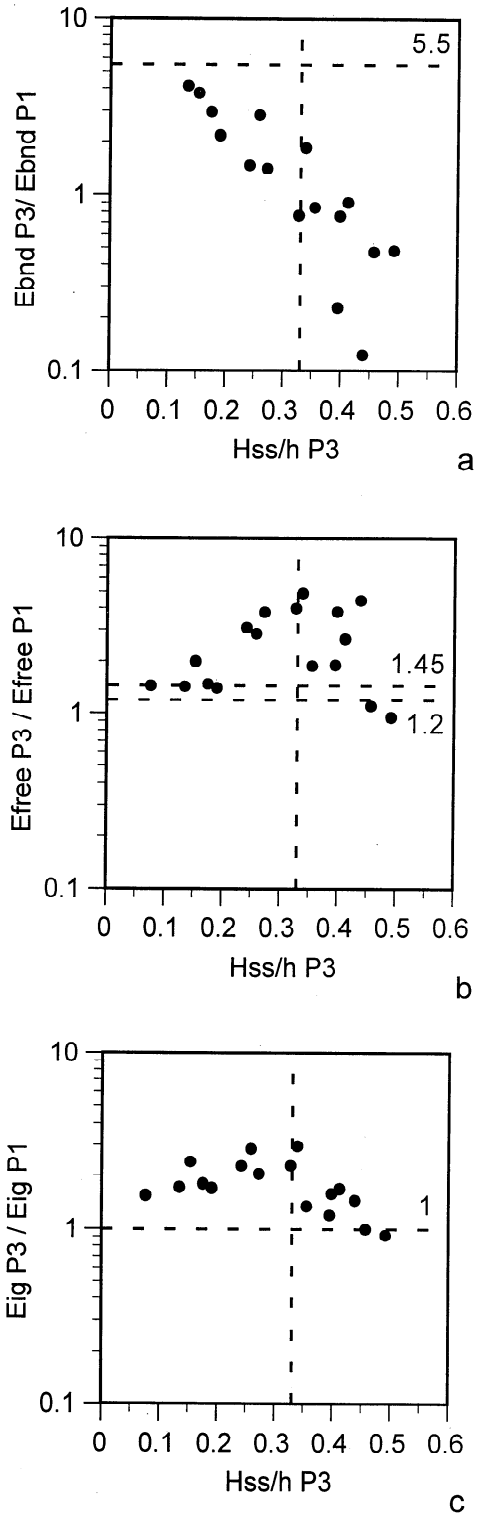

Figure 6. Cross-shore amplification of (a) bound, (b) free, and (c) total infragravity energy between P1 and P3 as a function of relative wave height H_{ss}/h at P3. The dashed vertical line in each plot denotes the onset of wave breaking (H_{ss}/h = 0.33). The horizontal dashed lines are explained in the text.

Figure 7 shows four representative examples of the cross-shore evolution of the amount and composition of infragravity-wave energy. The first example (Figure 7a) is characteristic of low-energetic nonbreaking conditions ($H_{ss,0}$

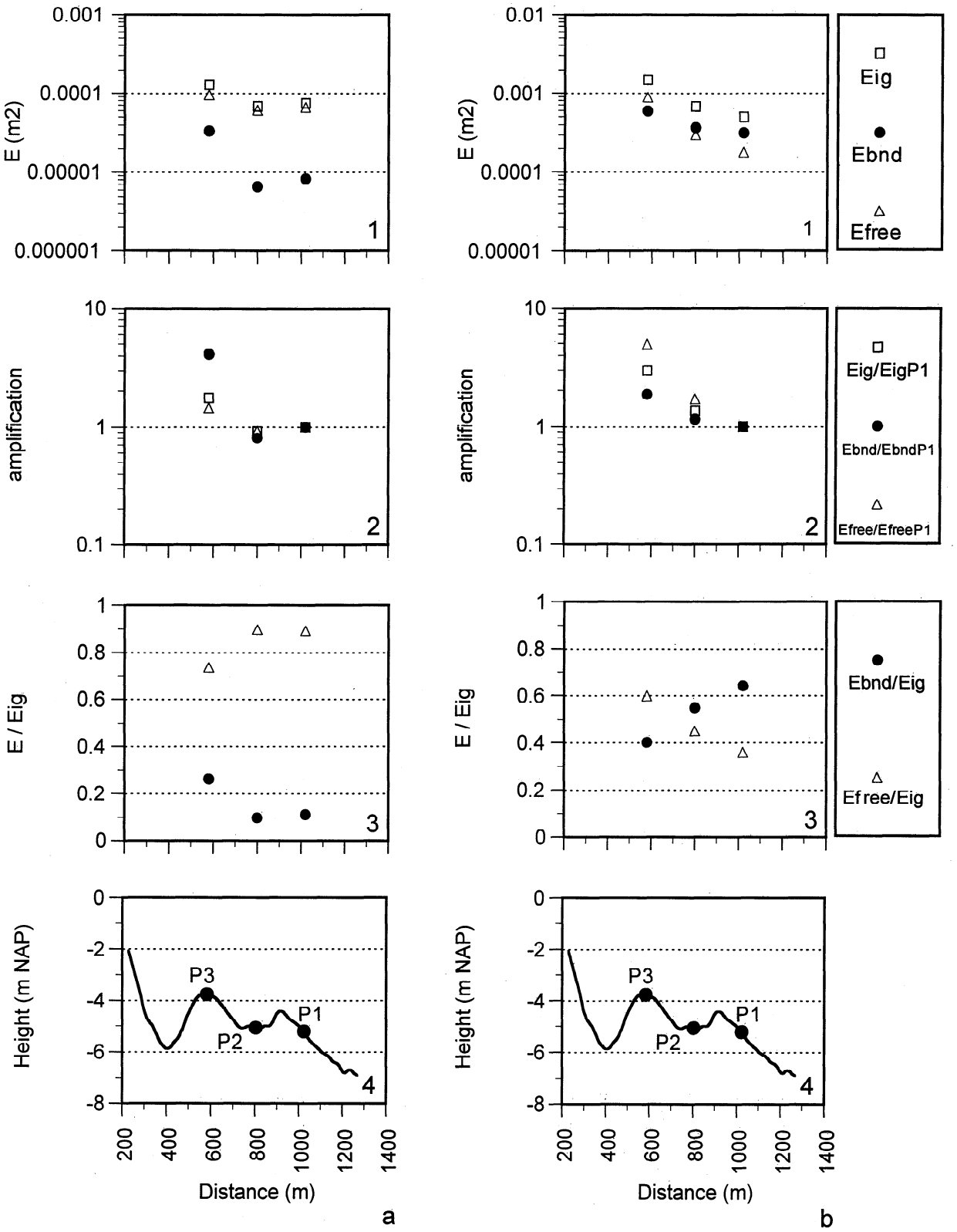

Figure 7. Representative examples of the cross-shore evolution of the amount and the composition of infragravity energy: (a) nonbreaking conditions ($H_{ss,o}$ = 0.7 m and H_{ss}/h at P3 = 0.13), (b) breaking at P3 ($H_{ss,o}$ = 1.1 m and H_{ss}/h at P3 = 0.34), (c) breaking at P1 ($H_{ss,o}$ = 2.6 m and H_{ss}/h at P1 = 0.34), and (d) well inside the surf zone ($H_{ss,o}$ = 3.9 m and H_{ss}/h at P1 = 0.47). The top plots show total, bound, and free infragravity energy. The second plots present the cross-shore amplification of total, bound, and free infragravity energy. The dashed lines denote equal amounts of energy at the various positions. The third plots show the local ratio of bound and free to total infragravity energy. The measurement profile is shown in the fourth plots as a cross-shore reference.

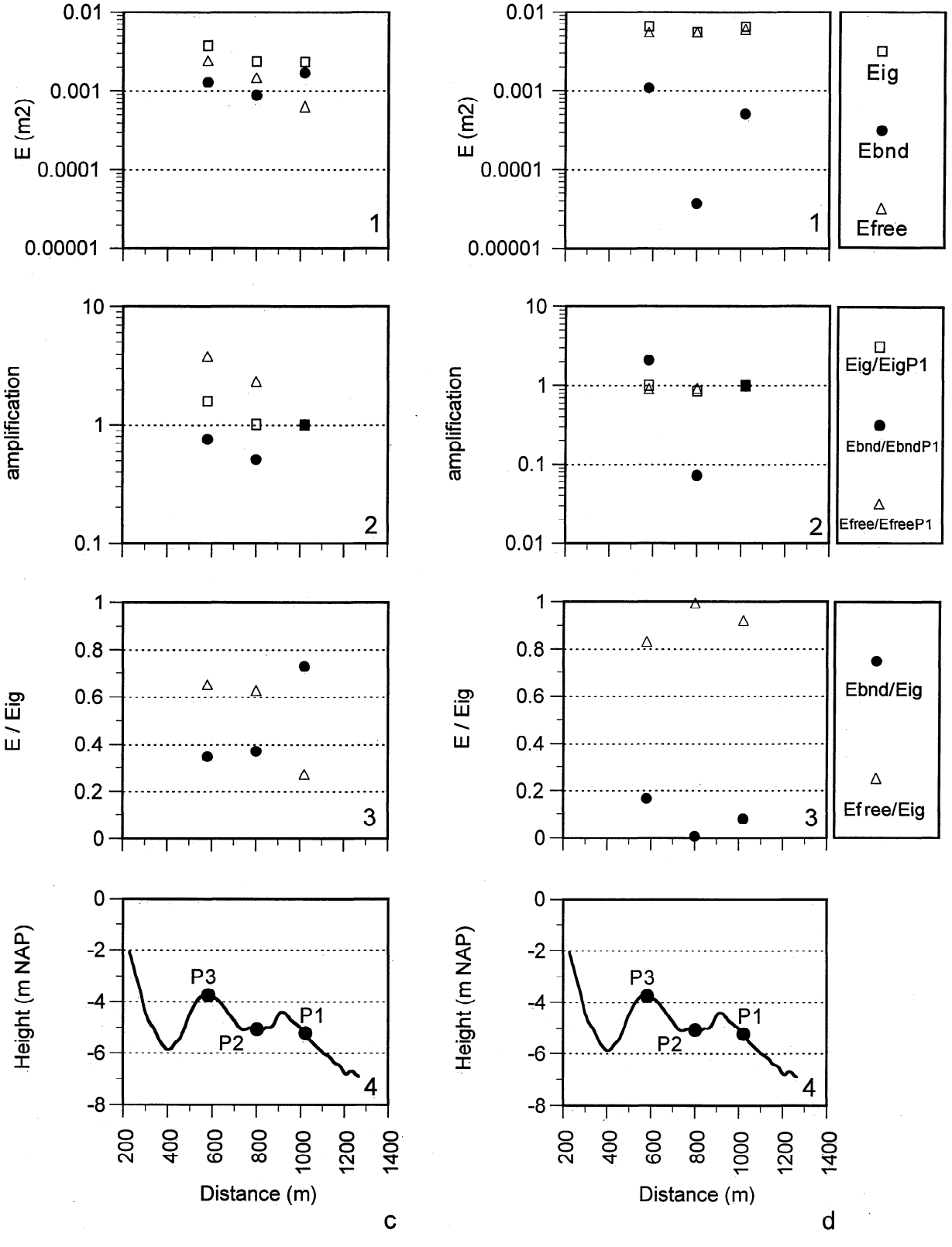

Figure 7. (continued)

= 0.7 m and H_{ss}/h at P3 = 0.13). Under these conditions, free waves dominated the total long-wave field; at the shallowest position (P3) the fraction of bound wave motions was larger than at the other positions (third plot). The shoaling characteristics of the free long waves were close to the theoretical value $(h^{P3}/h^{P1})^{-0.5}$ = 1.4 (low water) for leaky waves (second plot, see also Figure 6b). During the measurement shown in Figure 7b ($H_{ss,o}$ = 1.1 m), wave breaking took place at P3 (H_{ss}/h at P3 = 0.34). Despite the onshore growth in E_{bnd} the fraction of bound to total infragravity decreased in

the onshore direction, presumably related to the generation of free infragravity waves unrelated to short-wave breaking. Thus the ratio E_{bnd}/E_{ig} was not largest at the breakpoint spatially (third plot). In other words, forced waves contributed more substantially to the total long-wave field at P1 than at P3 despite the fact that the onset of short-wave breaking was located at the latter position.

During the example shown in Figure 7c, the outer breakpoint was located close to P1 ($H_{ss,o}$ = 2.6 m and H_{ss}/h at P1 = 0.34). As can be seen in the top two plots, E_{bnd} inside the surf zone was less than at P1, suggesting that spatially E_{bnd} reached maximum values at the onset of short-wave breaking (in contrast to E_{bnd} normalized by E_{ig}, as shown in Figure 7b, see also Figures 5a and 6a). The cross-shore change in the composition of the infragravity-wave field (third plot) was comparable to the previous, nonbreaking case; however, the transition from a dominance of forced to free motions was more marked because of the breaking-associated release over the outer bar. When the entire measurement transect experienced surf zone conditions (Figure 7d, $H_{ss,o}$ = 3.9 m and H_{ss}/h at P1 = 0.47), free wave motions were the dominant source of infragravity-wave energy (third plot), similar to the low-energy conditions in Figure 7a; however, their energy, just as the total infragravity-wave energy, amplified less than expected on account of the $h^{-0.5}$ dependence for leaky waves. Moreover, it even slightly reduced in the onshore direction (second plot, see also Figures 5 and 6), indicating a significant damping of infragravity energy under breaking conditions. The scatter in E_{bnd} and associated ratios is likely caused by the considerable uncertainties in the bispectral calculations when the coupling between the incident and infragravity waves is small (see Figure 4).

5. Discussion

The findings of the present measurements performed under nonbreaking conditions showed that forced motions became a more prominent constituent of the total infragravity-wave field with increasing short-wave height and decreasing depth, consistent with previous observations in deeper ($h \approx$ 10 - 30 m) water [e.g., *Bowers*, 1992; *Elgar et al.*, 1992; *Herbers et al.*, 1994; *Okihiro et al.*, 1992]. As, however, the present experiments were conducted in depths of only 2.5 to 7 m, the relative importance of forced and free long-wave motions to the total infragravity field could additionally be investigated through the onset of wave breaking all the way to the saturation of the short-wave field. The data set indicates (Figure 3) that at a given position the ratio of forced to total infragravity energy was largest at the beginning of breaking and subsequently diminished with increasing breaking intensity to negligible values in a saturated wave field. The strong coupling at the breakpoint between incident and infragravity waves with a phase relationship close to bound-wave theory strongly supports *Longuet-Higgins and Stewart*'s [1962] hypothesis that free infragravity waves are surf zone generated by the release of forced long waves.

The observed ratios of bound to total infragravity energy are not necessarily representative of other beaches. *Herbers et al.* [1995b] demonstrated convincingly that the amount of free long-wave energy is influenced by the geographical setting: the topography surrounding the measurement location determines the amount of reflection, dissipation as well as trapping. However, bound-wave energy is only a function of local parameters: water depth and short-wave characteristics.

In this paper the value H_{ss}/h = 0.33 has been used to mark the onset of short-wave breaking for all measurements at every location. It is well known that the value of H_{ss}/h marking saturation (hereafter referred to as γ) is slope dependent with larger values on steeper slopes [e.g., *Sallenger and Holman*, 1985; *Lippmann et al.*, 1996; *Raubenheimer et al.*, 1996]. Analogously, the H_{ss}/h value for which the highest waves start to break may depend on the local bottom slope as well. As the local bottom gradients at the Terschelling field site are small (generally less than 1:50), the range of γ values over the profile is expected to be minimal. Besides the slope dependence, several wave energy transformation models incorporate an effect of the offshore wave steepness on γ as well [e.g., *Battjes and Stive*, 1985; *Van Rijn and Wijnberg*, 1996], with steeper waves allowing larger maximum ratios of wave height to water depth. However, most results from field observations indicate that either the γ dependence on offshore wave steepness is absent [e.g., *Sallenger and Holman*, 1985; *Raubenheimer et al.*, 1996] or very weak [*Lippmann et al.*, 1996]. On the whole, the choice of H_{ss}/h = 0.33 as the start of short-wave breaking is justified for the measurements at P1, P2, and P3. As noted in section 2, the best value to know whether P2 was shoreward of the outer breaker zone was that at the outer bar crest. Nevertheless, the local relative wave height at P2 was applied. Judging from the trends shown in section 4 (e.g., at which H_{ss}/h value the ratio of bound to total infragravity energy reached its maximum), this choice did not seriously affect the outcome for P2.

6. Conclusions

Under nonbreaking conditions, bound infragravity energy levels in 2.5- to 7-m water depth are related to the offshore short-wave energy squared ($E_{bnd} \propto E_{ss,o}^2$), whereas in the $E_{ss,o}$ dependence of free infragravity energy the exponent is less than 1 (Table 1). Under surf zone conditions, E_{bnd} remains about constant or even drops off with a further increase in $E_{ss,o}$; in contrast, E_{free} then rapidly increases. The temporal variations in the contribution of forced to total infragravity energy are well linked to the local relative wave height (Figure 3). At a given cross-shore position, E_{bnd}/E_{ig} increases under more energetic conditions and smaller depths, reaching maximum values at the onset of wave breaking. With a growing breaking intensity the coupling between infragravity and short waves reduces and is negligible in a fully saturated wave field. The biphase is close to 180°, which, together with the strong phase coupling observed at the breakpoint, strongly supports the hypothesis that free infragravity waves are generated by the release of forced motions during short-wave breaking.

In the cross-shore direction the amount of forced infragravity energy is largest at the breakpoint. Wave breaking is associated with a rapid reduction in the contribution of bound to total infragravity energy in the onshore direction; consequently, the ratio between free and total infragravity energy rapidly increases (Figure 7c). The data set further indicates that free infragravity energy may also be generated in the absence of breaking waves (Figures 5b and 6b); the reason for this is not fully understood. This additional generation of free infragravity energy may cause the ratio E_{bnd}/E_{ig} to decrease in the onshore direction despite an onshore growth in E_{bnd} (Figure 7b).

Acknowledgments. Part of this work was supported by the NOURTEC project, Innovative Nourishment Techniques Evaluation, which was jointly funded by the Ministry of Transport, Public Works and Water Management in the Netherlands and by the Commission of the European Communities, Directorate General for Science, Research and Development under the Marine Science and Technology programme contract MAS2-CT93-0049. I would like to thank Thomas Herbers (Naval Postgraduate School, Monterey, California) for providing the bispectral source code and for his many useful suggestions during the analysis. In addition, his remarks made on a draft version of this paper were of great importance to me. The comments received from the anonymous reviewers are greatly appreciated.

References

Battjes, J.A., and M.J.F. Stive, Calibration and verification of a dissipation model for random breaking waves, *J. Geophys. Res.*, *90*, 9159-9167, 1985.

Bowers, E.C., Low frequency waves in intermediate water depths, in *Proceedings of the 23rd International Conference on Coastal Enginering*, pp. 832-845, Am. Soc. of Civ. Eng., Reston, Va., 1992.

Eldeberky, Y., and J.A. Battjes, Nonlinear coupling in waves propagating over a bar, in *Proceedings of the 24th International Conference on Coastal Engineering*, pp. 157-167, Am. Soc. of Civ. Eng., Reston, Va., 1994.

Eldeberky, Y., and J.A. Battjes, Spectral modeling of wave breaking: application to Boussinesq equations, *J. Geophys. Res.*, *101*, 1253-1264, 1996.

Elgar, S., and R.T. Guza, Observations of bispectra of shoaling surface gravity waves, *J. Fluid Mech.*, *161*, 425-448, 1985.

Elgar, S., and G. Sebert, Statistics of bicoherence and biphase, *J. Geophys. Res.*, *94*, 10993-10998, 1989.

Elgar, S., T.H.C. Herbers, M. Okihiro, J. Oltman-Shay, and R.T. Guza, Observations of infragravity waves, *J. Geophys. Res.*, *97*, 15573-15577, 1992.

Guza, R.T., and A.J. Bowen, Resonant interactions for waves breaking on a beach, in *Proceedings of the 15th International Conference on Coastal Engineering*, pp. 560-579, Am. Soc. of Civ. Eng., Reston, Va., 1976.

Hasselmann, K., On the non-linear energy transfer in a gravity-wave spectrum, 1, General theory, *J. Fluid Mech.*, *12*, 481-500, 1962.

Hasselmann, K., W. Munk, and G. MacDonald, Bispectra of ocean waves, in *Time Series Analysis*, edited by M. Rosenblatt, pp. 125-139, John Wiley, New York, 1963.

Herbers, T.H.C., S. Elgar, and R.T. Guza, Infragravity-frequency (0.005-0.05 Hz) motions on the shelf, I, Forced waves, *J. Phys. Oceanogr.*, *24*, 917-927, 1994.

Herbers, T.H.C., S. Elgar, and R.T. Guza, Generation and propagation of infragravity waves, *J. Geophys. Res.*, *100*, 24863-24872, 1995a.

Herbers, T.H.C., S. Elgar, R.T. Guza, and W.C. O'Reilly, Infragravity-frequency (0.005-0.05 Hz) motions on the shelf, II, Free waves, *J. Phys. Oceanogr.*, *25*, 1063-1079, 1995b.

Hoekstra, P., K.T. Houwman, A. Kroon, P. van Vessem, and B.G. Ruessink, The Nourtec experiment of Terschelling: Process-oriented monitoring of a shoreface nourishment (1993-1996), in *Proceedings of Coastal Dynamics'94*, pp. 402-416, Am. Soc. of Civ. Eng., Reston, Va., 1994.

Holman, R.A., Infragravity energy in the surf zone, *J. Geophys. Res.*, *86*, 6442-6450, 1981.

Howd, P.A., J. Oltman-Shay, and R.A. Holman, Wave variance partitioning in the trough of a barred beach, *J. Geophys. Res.*, *96*, 12781-12795, 1991.

Huntley, D.A., R.T. Guza, and E.B. Thornton, Field observations of surf beat, 1, Progressive edge waves, *J. Geophys. Res.*, *86*, 6451-6466, 1981.

Lippmann, T.C., A.H. Brookins, and E.B. Thornton, Wave energy transformation on natural profiles, *Coastal Eng.*, *27*, 1-20, 1996.

List, J.H., A model for the generation of two-dimensional surf-beat, *J. Geophys. Res.*, *97*, 5623-5635, 1992.

Longuet-Higgins, M.S., and R.W. Stewart, Radiation stress and mass transport in surface gravity waves with application to "surf beats," *J. Fluid Mech.*, *13*, 481-504, 1962.

Munk, W.H., Surf beat, *Eos Trans. AGU*, *30*, 849-854, 1949.

Okihiro, M., R.T. Guza, and R.J. Seymour, Bound infragravity waves, *J. Geophys. Res.*, *97*, 11453-11469, 1992.

Oltman-Shay, J., and R.T. Guza, Infragravity edge wave observations on two California beaches, *J. Phys. Oceanogr.*, *17*, 644-663, 1987.

Raubenheimer, B., R.T. Guza, and S. Elgar, Wave transformation across the inner surf zone, *J. Geophys. Res.*, *101*, 25589-25597, 1996.

Ruessink, B.G., and A. Kroon, The behaviour of a multiple bar system in the nearshore zone of Terschelling, the Netherlands: 1965-1993, *Mar. Geol.*, *121*, 187-197, 1994.

Sallenger, A. H., Jr., and R.A. Holman, Wave energy saturation of a natural beach of variable slope, *J. Geophys. Res.*, *90*, 11939-11944, 1985.

Symonds, G., D.A. Huntley, and A.J. Bowen, Two-dimensional surf beat: Long wave generation by a time-varying breakpoint, *J. Geophys. Res.*, *87*, 492-498, 1982.

Thornton, E.B., and R.T.Guza, Energy saturation and phase speeds measured on a natural beach, *J. Geophys. Res.*, *87*, 9499-9508, 1982.

Tucker, M.J., Surfbeats: Sea waves of 1 to 5 minutes' period, *Proc. R. Soc. London A*, *202*, 565-573, 1950.

Van Enckevort, I., and E. Reincke, Longshore currents in the intertidal zone of Terschelling, M.Sc. thesis, *IMAU Report V96.09*, Utrecht University, 62 pp., 1996.

Van Rijn, L.C., and K.M. Wijnberg, One-dimensional modelling of individual waves and wave-induced longshore currents in the surf zone, *Coastal Eng.*, *28*, 121-145, 1996.

B.G. Ruessink, Institute for Marine and Atmospheric Research Utrecht, Department of Physical Geography, Utrecht University, P.O. Box 80.115, 3508 TC Utrecht, Netherlands. (e-mail: b.ruessink@frw.ruu.nl)

(Received March 25, 1997; revised October 30, 1997;
accepted February 12, 1998.)